Micelle Formation by a Fragment of Human Islet Amyloid Polypeptide

Elizabeth Rhoades*† and Ari Gafni*†‡
*Biophysics Research Division, †Institute of Gerontology, and ‡Department of Biological Chemistry, University of Michigan, Ann Arbor, Michigan 48109

ABSTRACT Human islet amyloid polypeptide (hIAPP) is the major component of amyloid plaques found in the pancreatic islets of persons with type 2 diabetes mellitus. HIAPP belongs to the group of amyloidogenic proteins, characterized by their aggregation and deposition as fibrillar amyloid in various body tissues. The aggregation of amyloidogenic proteins is thought to occur via a common pathway, but currently no unifying kinetic model exists. In previous work, we presented a model of amyloid fibril formation formulated from our observations of the aggregation of an amyloidogenic fragment of hIAPP, amino acids 20–29. Our model is based on nucleation-dependent aggregation, modified by the formation of off-pathway hIAPP micelles. In the present study we confirm the presence of peptide micelles, and experimentally determine the critical micelle concentration in solutions of hIAPP fragments using three different techniques: conductivity, pH, and fluorescence. All three techniques yield a critical micelle concentration of 3–3.5 μM peptide. Furthermore, based on changes in the fluorescence intensity of a labeled peptide fragment as well as a decrease in solution pH as a result of deprotonation of the amino terminus, we conclude that the amino terminus of the fragment undergoes a significant change of environment upon micellization.

INTRODUCTION

One of the significant pathologies of type 2 diabetes mellitus (type 2 DM) is the formation of extracellular amyloid deposits in the β-cells of the islets of Langerhans in the pancreas (Johnson et al., 1988; Westermark and Wilander, 1978). The primary component of these deposits is human islet amyloid polypeptide (hIAPP) (Cooper et al., 1987), a 37-amino acid peptide hormone that is normally produced in, and secreted from, the β-cells, and functions to control hyperglycemia by regulating the rate at which dietary glucose enters the blood stream. The causal relationship between type 2 DM and the development of hIAPP amyloid deposits has not yet been proven, though it is known that sites of hIAPP amyloid deposition are surrounded by β-cell degeneration and that solutions containing hIAPP fibrils formed in vitro are toxic to cultured human and rat islet β-cells (Lorenzo et al., 1994).

HIAPP is one of a growing number of proteins and peptides that are classified as amyloidogenic, referring to the amyloid plaques formed by their deposition as highly ordered aggregates in the tissues of persons affected by one of a variety of diseases. The mechanism of fibril formation and the general structure of the fibrils are thought to be common to all amyloidogenic proteins. The initial aggregates formed are slender, unbranched fibers that range from 3- to 8-nm in diameter and up to several 100-nm in length (Goldsbury et al., 1997; Harper et al., 1997b). Atomic force and electron microscopies have been used to follow the self-assembly of the elementary fibrils to form a variety of differently structured mature fibrils, dependent upon such factors as solvent conditions and the particular amyloidogenic protein involved (Charge et al., 1995; Goldsbury et al., 2000; 1997; Harper et al., 1997a,b). The mature fibrils are characterized by intermolecular antiparallel β-sheets, oriented roughly perpendicular to the axis of the fibers, as seen with circular dichroism, nuclear magnetic resonance, and x-ray diffraction (Blake and Serpell, 1996; Cohen and Calkins, 1959; Cort et al., 1994; Griffiths et al., 1995; Kirschner et al., 1986; Sunde et al., 1997).

To gain a full understanding of the process of amyloid formation, it is crucial not only to characterize the structure of the fibrils, but also to develop a kinetic model that describes how these fibrils are formed. There is significant evidence that amyloid fibril formation is a nucleation-dependent process (Ashburn et al., 1992; Jarrett and Lansbury, 1992, 1993; Lomakin et al., 1996) (depicted in Fig. 1 *A*) and thereby resembles other ordered protein aggregation processes such as protein crystallization (Blow et al., 1994), sickle cell hemoglobin polymerization (Mirchev and Ferrone, 1997), and viral coat protein assembly (Schuster et al., 1979). The nucleation-dependent aggregation process is initiated by the forming of a nucleus, defined as the smallest, marginally stable, structured aggregate created by the concerted association of monomers. Because there is a high entropic barrier to nucleation, it is the rate-limiting step in the aggregation process, giving rise to a distinct lag time before aggregation is initiated. However, once a nucleus is formed, the addition of monomers to the growing aggregate is favorable (in Fig. 1 *A*, $K_b \gg K_a$) and aggregation proceeds rapidly. Since nucleation is a high-order reaction, it is expected to depend strongly upon the concentration of the protein. More precisely, for a nucleus consisting of j-monomers, the lag time is expected to be inversely proportional to the total protein concentration to the $(j + 1)th$

Submitted September 10, 2002, and accepted for publication December 9, 2002.

Address reprint requests to Dr. Ari Gafni, Biophysics Research Div., University of Michigan, 930 N. University Ave., Ann Arbor, MI 48109-1055. Tel.: 734-936-2156; Fax: 34-936-2116; E-mail: arigafni@umich.edu.

Dr. Rhoades' present address is Weizmann Institute of Science, Dept. of Chemical Physics, Rehovot 76100, Israel.

0006-3495/03/05/3480/08 $2.00

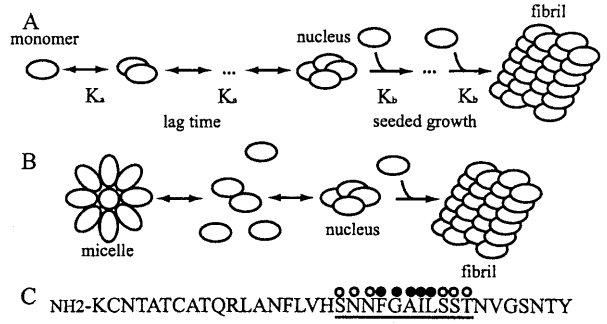

FIGURE 1 (*A*) Schematic representation of nucleation-dependent aggregation. The nucleus forms from the slow association of *j*-monomers. Its rate of formation thus depends on the $(j + 1)th$ power of the monomer concentration. In contrast, the addition of monomers to the nucleus or to the growing polymers is favorable and proceeds rapidly (adapted from Jarrett and Lansbury, 1993). (*B*) Schematic representation of nucleation-dependent aggregation with off-pathway micelles. Above the critical micelle concentration, monomers and micelles exist in a rapid equilibrium that maintains a constant monomer concentration. The nucleus is formed from monomer peptide-peptide interactions. (*C*) Amino acid sequence of human islet amyloid polypeptide, with amino acids 20–30 underlined, hydrophilic residues marked with open circles, and hydrophobic residues marked with solid circles.

power (Oosawa and Kasai, 1962). Thus, small changes in the total protein concentration result in dramatic changes in the aggregation lag time, even for nuclei consisting of only three or four monomers. A striking example is the initiation of sickle cell hemoglobin polymerization, which is highly concentration-dependent, so that a twofold dilution of the protein concentration prolongs the lag time some 10-billion-fold (Ferrone et al., 1985). The lag phase can be eliminated by the addition of preformed nuclei, or seeds, to a monomeric protein solution.

Describing the kinetics of aggregation of amyloidogenic peptides and quantification of intermediates on the aggregation pathway has proven to be challenging for two major reasons. The first reason is that to accurately describe early stages in the aggregation process, initial peptide solutions must be fully monomeric, as it has been shown by many groups that the presence of even a small amount of seed material results in immediate aggregation of the peptide (Come et al., 1993; Jarrett and Lansbury, 1993; Snyder et al., 1994; Wood et al., 1996). Despite this, relatively few studies have emphasized this point or made serious efforts to ensure fully monomeric solutions (Jarrett and Lansbury, 1992; Rhoades et al., 2000; Walsh et al., 1999). Not only do the seeds eliminate the initial stages of aggregation (nucleation), they also make it difficult to obtain reproducible initial conditions, as varying amounts of seeds may be found in different preparations. The second reason is that many methods traditionally used to follow amyloid formation, such as turbidity or dye binding, are incapable of detecting early intermediates. Since these aggregation intermediates are small, and usually present in low concentrations, they are frequently below the threshold of detection by turbidity. Likewise, if the intermediates have different secondary structures than the mature fibrils, then dyes such as Congo Red and Thioflavin T, which bind to the interstrand β-sheets of the mature fibrils, will not detect these intermediates. A number of kinetic models based on dynamic light scattering have been proposed for the aggregation of the amyloidogenic peptide associated with Alzheimer's disease, Aβ (Lomakin et al., 1996, 1997; Pallitto and Murphy, 2001; Tomski and Murphy, 1992), but a general model is still lacking.

In our previous work, we focused on characterizing the initiation of aggregation of a fragment of hIAPP in terms of its lag time before detectable aggregation occurs (Rhoades et al., 2000). We found that for a wide range of peptide concentrations, $\sim$5 μM–150 μM, under conditions where we were confident that our initial solutions contained only monomeric peptide, the lag time was independent of the total concentration of the peptide, in direct contradiction to what is predicted for nucleation dependent aggregation. To explain our observations, we developed a modified model of nucleation-dependent aggregation, shown in Fig. 1 *B*. In this model, off-aggregation-pathway peptide micelles are formed at peptide concentrations greater than the critical micelle concentration (CMC). The formation of micelles helps maintain the monomer concentration at the CMC since whenever the total peptide concentration exceeds the CMC, all excess peptide is incorporated into micelles. Nuclei are formed only from monomeric peptide interactions, as in the classic nucleation-dependent aggregation model (Fig. 1 *A*), and thus nucleation depends only on the concentration of monomeric peptide. Therefore, for concentrations greater than the CMC, the lag time does not exhibit a dependence upon the total protein concentration. If the micelles were on-pathway (i.e., they give rise to nuclei), then we would expect to see some dependence of the lag time upon the peptide concentration, as explained in the following. An increase in the peptide concentration results in an increase in the number of micelles in solution. A higher concentration of micelles results in more rapid nucleus formation, and a consequent decrease in the lag time to aggregation. However, as we do not see a dependence of the lag time upon the concentration of peptide, then the micelles must be off-pathway. Further evidence that our model may serve as the basis for a general one describing amyloid aggregation comes from recent kinetic studies which show that the aggregation of full-length hIAPP (Padrick and Miranker 2002), as well as prion protein Sup 35 (Serio et al., 2000), are concentration-independent.

The presence of off-pathway peptide micelles is a key, but hitherto unproven, component of our hIAPP aggregation model (Fig. 1 *B*). Thus, the aim of this study was to experimentally test for the presence of hIAPP micelles in solution using approaches that have been previously applied for the characterization of conventional micelle-forming solutions. It is well established that many physiochemical properties of such solutions change abruptly at the CMC (Hiemenz

and Rajogopalan, 1997), including but not limited to: light scattering, viscosity, surface tension, absorption, fluorescence, conductivity, and pH. To determine the CMC of a micelle-forming substance, one of these properties is monitored as a function of concentration and a change in the slope of the plot made from the data marks the CMC.

In the study presented here, we confirm the presence of micelles formed by hIAPP fragments in solution, and determine the CMC with three independent techniques: conductivity, pH, and fluorescence intensity. Three fragments of hIAPP were used: amino acids 20–30 (hIAPP 20–30), 20–29 with a tryptophan (Trp) at the carboxyl terminus (hIAPP 20–29-Trp), and 20–29 with a fluorescein at the amino terminus (hIAPP fluo-20–29). Previous studies have established that hIAPP fragments containing residues 20–29 may serve as suitable model systems for in vitro amyloid formation since these fragments are capable of forming amyloid fibrils in vitro that are indistinguishable from (and exhibit many of the amyloidogenic characteristics of) fibers formed by the full-length peptide (Fig. 1 *C*) (Ashburn et al., 1992; Charge et al., 1995; Glenner et al., 1988; Westermark et al., 1990). The tryptophan and fluorescein groups were added to two of the fragments to serve as fluorescent probes of the carboxyl and amino termini, respectively.

MATERIALS AND METHODS

The fragments hIAPP 20–30, hIAPP 20–29-Trp, and rat IAPP 20–29 (rIAPP 20–29) were synthesized by the Protein and Carbohydrate Core Facility (University of Michigan, Ann Arbor) and were purified by reversed-phase high-performance liquid chromatography to >98% purity. hIAPP fluo-20–29 was purchased from Bio-Synthesis Incorporated (Lewisville, TX). Though these peptide fragments show slight differences in their solubilities, turbidity measurements show that the aggregation of each of these peptides is concentration-independent between ~5 and 150 μM, and characterized by a lag phase of ~40 h before detectable aggregation. This behavior corresponds to our previously published data (not shown) (Rhoades et al., 2000). Moreover, at the concentration range used, the length of this lag phase was concentration-independent. Experiments were repeated a minimum of five times, and the data presented here is the average of at least five experiments.

The hIAPP fragments were dissolved in 100% dimethyl sulfoxide (DMSO) to create stock solutions of 20 mM. The stock solutions were stored at −20 C. When needed, the necessary amount of peptide was removed from the DMSO stock and diluted into 25 μM KCl. The concentration of DMSO is 0.1% throughout all the experiments, which did not affect the aggregation of the fragments (data not shown). The solutions were filtered through a 0.2-μm Acrodisc syringe filter (Pall Gelman Sciences, Ann Arbor, MI) to remove dust and other particulate matter.

Conductivity measurements were made using a Cole-Parmer Digital conductivity meter, with a gold-plated dip cell with a built-in thermistor (Vernon Hills, IL). The pH of the solutions was measured indirectly by using a pH-sensitive dye, Bromcresol Purple (BP), from Sigma Chemical Company (St. Louis, MO). The absorption spectrum of BP changes over a range of pH 5.2–6.8 which we found to be suitable for our experiments. Absorption measurements of the BP/hIAPP fragment solutions were made with a Shimadzu UV-Vis spectrophotometer and the ratio Abs587/Abs430, which is particularly sensitive to pH changes, was used. Fluorescence emission measurements of hIAPP 20–29-Trp and hIAPP fluo-20–29 were made with a Spex model Fluorolog II fluorimeter. The hIAPP 20-29-Trp was excited at 290 nm and the emission from 300 to 400 nm was recorded. The hIAPP fluo-20–29 was excited at 465 nm and the emission collected from 475 to 600 nm. All measurements were made at room temperature.

A 20-μM solution of the appropriate hIAPP fragment was prepared by diluting 1 μl of the 20-mM stock solution into 1 mL of 25 μM KCl. As we mention in the Introduction, our previous work characterized the aggregation of hIAPP fragment solutions over a range of concentrations for 5 μM to 150 μM, finding that these solutions remained kinetically soluble for a period of ~40 h. However, these solutions were prepared by diluting the stock solutions of hIAPP fragments in DMSO into 10 mM sodium phosphate buffer pH 7, with 10 mM NaCl. For the studies presented here, we use ddH_2O rather than buffer, as buffer interferes with both the conductivity and pH measurements. Thus we chose 20 μM as the highest peptide concentration because it was determined that this value represents the solubility limit of the hIAPP fragments in pure ddH_2O. Higher concentrations of peptide diluted into ddH_2O resulted in irreproducible behavior, and often in rapid, visible, insolubilization of the peptide. The measurements of conductivity, absorption, and fluorescence were carried out in one of the following two ways: 1), A measurement of the signal from a peptide solution was made, then the sample was diluted to the next desired concentration with 25 μM KCl/0.1% DMSO. And 2), Each concentration was prepared by direct dilution of the initial 20 μM peptide solution to the desired concentration and each sample was then measured. Both methods gave comparable, reproducible results. The dilutions were repeated until the concentration was too low for reproducible measurements to be obtained. For the absorption studies, 2 μL of a 5-mM stock of BP were added to 1 mL of the 20-μM peptide solution, for a final dye concentration of 10 μM. These samples were diluted with 25 μM KCl/0.1% DMSO/10 μM BP. We observe that solutions of 20 μM hIAPP in ddH2O or 25 μM KCl are kinetically soluble (i.e., no detectable seeds or aggregates form) for close to 40 h. As all measurements were made within an hour after diluting the peptide stocks into aqueous solution, we do not expect seed formation or aggregation to be an issue for either serially diluted or directly diluted solutions.

RESULTS

Fresh solutions of hIAPP 20–30, hIAPP 20–29-Trp, and hIAPP fluo-20–29, prepared as described in Materials and Methods, were free of all amyloidogenic material as verified by their reproducible aggregation behavior, explained in detail in our previous work (Rhoades et al., 2000). As mentioned, under our experimental conditions, we consistently observed a lag time of ~40 h for the hIAPP fragment, confirming that the solutions were initially free from nuclei and other amyloidogenic material.

Fig. 2 shows the conductivity of hIAPP 20–30 solutions as a function of peptide concentration. The CMC, which is particularly clearly marked by a change in slope from positive to negative (see Discussion), is ~3.5 μM. As will be discussed later, the shape of the conductivity curve of hIAPP 20–30 in 25 μM KCl resembles the conductivity curve of sodium dodecyl sulfate (SDS), a well-characterized micellar system, in 6 mM HCl. The conductivity of solutions of rIAPP 20–29 (which does not aggregate) was measured as a control, with no evidence of micelles observed (data not shown).

BP absorption ratio versus peptide concentration is shown in Fig. 3. As with the conductivity measurements, a clear change in slope is observed, and the CMC value determined from this break is ~3 μM, in very good agreement with the conductivity data. Although the data is plotted as absorbance

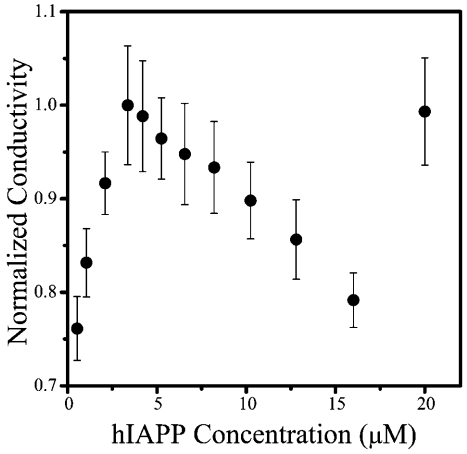

FIGURE 2 Conductivity as a function of hIAPP 20–30 concentration. The change in slope of the curve at ~3.5 μM is interpreted as the CMC of the solution.

ratio of BP, these values correspond to the changing pH of the solutions, i.e., an increase in the absorbance ratio corresponds to a decrease in solution pH. It is clear from Fig. 3 that the slope of the absorption ratio versus peptide concentration is larger above the CMC than below this value. This indicates that the pH decreases more rapidly at concentrations above the CMC, where the micelle concentration increases with increasing peptide concentration while the monomer concentration remains constant. The micellization, therefore, is associated with an increase in H^+ ions released into solution. If the change in pH observed for hIAPP 20–30 solutions were merely due to a change in the ionic strength of the unbuffered solution (due to, for example, an increase in the amount of salt from the lyophilized peptide, proportional to the increasing amount of peptide), then one would expect the relationship between concentration and pH to be a simple linear one.

The data in Fig. 4 shows the change in the fluorescence intensity of the fluorescein and tryptophan-labeled hIAPP 20–29 as a function of peptide concentration. The emission intensity of hIAPP fluo-20–29 reveals a definite change in the slope at ~3 μM peptide, also in very good agreement with both the conductivity and pH measurements. Furthermore, as the fluorescein serves as a probe of the amino terminus of the peptide, this data indicates that this terminus experiences a change in its environment upon micellization.

We cannot draw any definite conclusions from the data for hIAPP 20–29-Trp since the fluorescence intensity increases linearly with peptide concentration. This can be rationalized in two ways: 1), the carboxyl terminus does not change environment upon micellization; or 2), the tryptophan fluorescence is insensitive to changes in the chromophore's environment upon micellization.

DISCUSSION

Conductivity has been frequently used to determine the CMC of ionic solutions and is considered to be one of the most effective methods for doing so (Mukerjee and Mysels, 1971). Using this approach we measure a CMC of ~3.5 μM for hIAPP 20–30 in 25 μM KCl. As mentioned in Results,

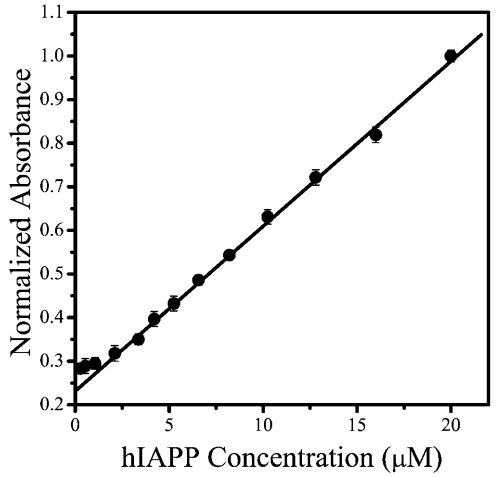

FIGURE 3 Bromcresol Purple absorption as a function of hIAPP 20–30 concentration. The absorbance values at 430 nm and 587 nm of the hIAPP 20–30/BP solutions are plotted as a normalized ratio absorbance (587 nm/430 nm). The CMC is ~3 μM, as determined by a change in the slope of the plot. Increasing normalized absorbance intensity is inversely proportional to pH: the solutions become more acidic with increasing hIAPP 20–30 concentration. The line shown is a linear fit to data from hIAPP concentrations >5 μM.

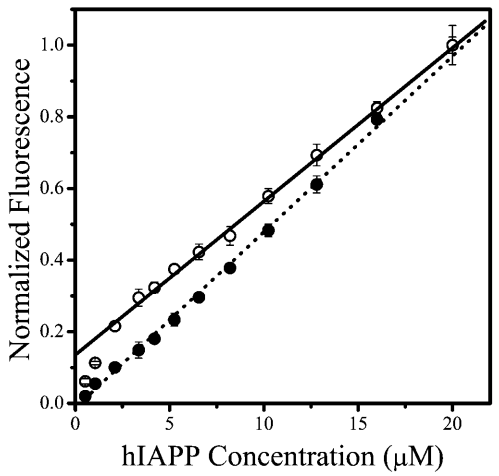

FIGURE 4 Fluorescence intensity of hIAPP fluo-20–29 (*open circles*) and hIAPP 20–29-Trp (*solid circles*) as a function of peptide concentration. The hIAPP fluo-20–29 was excited at 465 nm and the emission intensity at 515 nm is plotted. The hIAPP 20–29-Trp was excited at 290 nm and the emission intensity at 350 nm is plotted. The hIAPP fluo-20–29 shows a clear change in slope at ~3 μM peptide, indicating that the amino terminus undergoes a change in environment upon micellization. The line shown is a linear fit to the data from hIAPP fluo-20–29 concentrations >5 μM.

the shape of the curve closely resembles that of SDS in 6 mM HCl, for which equations have been derived and presented by Dominguez and co-workers (Dominguez et al., 1997). In their model, the change in slope of the conductivity versus concentration curve, from positive to negative, at the CMC is due to the fact that the forming SDS micelles carry a high density of negative charge on their surface and attract cations, thereby reducing their mobility and leading to decreased conductivity. This negative slope persists for a range of concentrations immediately above the CMC, but at higher concentrations, when cation capture is saturated, the slope reverts to a positive one. Our explanation of the results presented in Fig. 2 is that the behavior of the hIAPP 20–30 micelle system in presence of KCl is similar to that described by Dominguez and co-workers for SDS in presence of HCL, and thus that the equations presented by these authors can be used to describe our results. We refer the reader to the Dominguez and co-workers publication for a more detailed, quantitative, description of micellization in the presence of counterions. While we do not know the exact characteristics of the hIAPP micelles, i.e., how many monomers are associated, to what extent the micelles are ionized upon forming, what concentrations of counter ions associate with them, etc., the conductivity data shown in Fig. 2 clearly indicate the CMC value.

It is also important to mention that due to the nature of the hIAPP fragments, we were limited in the parameters we could vary in our conductivity measurements. As described in Materials and Methods, the solubility limit of hIAPP 20–30 in 25 μM KCl is $\sim$20 μM. Thus we were not able to measure the conductivity of solutions at higher concentrations, although we expect that the value should resume its increase. Additionally, we were unable to vary the KCl concentration substantially. At higher concentrations of KCl, the conductivity of this salt overwhelms that of the hIAPP fragments. We did attempt to measure the conductivity of hIAPP 20–30 in solutions with very low (5 μM) or no KCl. Though we found that these measurements were somewhat irreproducible (most likely due to the low concentrations of ions), the overall shape of the plots resembled conductivity plots of SDS in the absence of HCl: a line with a positive slope that changes at the CMC, to a line with a slightly lower, but still positive, slope (data not shown). Thus, the behavior of hIAPP 20–30, as measured by conductivity, in the absence and presence of KCl appears to be very similar to that of SDS in the absence and presence of HCl. This confirms that our conductivity measurements indeed report on the presence of hIAPP micelles in solution.

Though in Fig. 1 *B* we depict the micelles as resembling traditional amphipathic structures, at present we do not have a physical model for the overall shape or size of the micelles. We thus use the term ''micelle'' to loosely describe the structures formed by rapid, reversible, nonfibrillar oligomerization of the hIAPP fragment. During amyloid formation, as monomer peptide is depleted by being incorporated first into nuclei and then into growing fibrils, the micelles disassemble. The term ''micelle'' has been used to describe oligomeric structures formed by other amyloidogenic peptides. Before our work, Lomakin and co-workers used the term ''micelle'' to describe on-pathway oligomeric intermediates formed by the Alzheimer's Aβ peptide that give rise to nuclei and then fibrils (Lomakin et al., 1996, 1997). More recently, Serio and co-workers describe off-pathway oligomeric structures formed by the prion protein Sup35 as ''micellelike'' in their kinetics (Serio et al., 2000). Initial studies by both Harper et al. (1997b) and Walsh et al. (1997) proposed that one possible role for the oligomeric structures formed by Aβ, termed protofibrils, is to serve as off-pathway peptide reservoirs, kinetic entities much like our micelles. Thus, we use the term as a useful kinetic description and not necessarily to imply that the hIAPP 20–29 forms traditional micellar structures. We also use the term to emphasize the difference between off-pathway oligomers (the micelles) and other small oligomers, such as seeds or small aggregates that are found on-pathway.

The CMC we measured with conductivity was confirmed by pH/absorbance and fluorescence intensity measurements, both showing the CMC to be $\sim$3 μM. In addition to corroborating the conductivity measurements, these two techniques also yield some information about the structure of the micelles. From the pH/absorption we can determine that solutions of hIAPP 20–30 ($p\mathrm{K_a} \approx 5.5$) in 25 μM KCl are increasingly more acidic with increasing peptide fragment concentration. Above the CMC, the pH decreases more sharply, as indicated by an increase in the slope of the plot of BP absorbance versus hIAPP 20–30 concentration (Fig. 3). The increasing acidity indicates that enhanced release of H^+ ions into solution occurs upon micellization, an effect that has been previously observed with other micelle-forming peptides (Kumar et al., 1996; Mandal and Jayakumar, 1994). Because the fragment hIAPP 20–30 does not contain any titratable side groups (see Fig. 1 *C* for the amino acid sequence of hIAPP), the only likely candidates for deprotonation are the terminal amino and carboxyl groups. At neutral pH, the carboxyl groups ($p\mathrm{K_a} \sim 3.1$) are fully deprotonated, making the amino terminus the likely proton donor. A plausible explanation of this observation is that upon micellization, the amino termini of the peptide fragments come into close proximity with each other, resulting in a decrease of the $p\mathrm{K_a}$ of the NH_3^+ groups with consequent partial deprotonation of these groups, and a decrease in the pH of the solution.

The fluorescently-labeled peptides provide further evidence for the involvement of the amino terminus in the micellization. hIAPP fluo-20–29 and hIAPP 20–29-Trp were used to probe the environments of the amino and carboxyl termini, respectively, of the peptide. The linear relationship between the Trp fluorescence intensity and the peptide concentration indicates that the environment of the carboxyl terminus does not change significantly upon micellization.

Time-resolved fluorescence anisotropy data of hIAPP 20-29-Trp (data not shown) displays an extremely rapid decay, indicating that the Trp has free rotational movement in solution, and therefore that the carboxyl terminus is solvent-exposed. Conversely, the fluorescence of hIAPP fluo-20–29 indicates that the amino terminus does undergo a change of environment upon micellization. It is well known that fluorescein emission intensity sharply decreases upon removal from aqueous to less polar solvents. The data in Fig. 4 show that the fluorescence intensity per unit of hIAPP fluo-20–29 decreases above the CMC, as evidenced by a decrease in the slope of the plot. An explanation for this decrease is that the environment of the amino terminus in the micelle is not as polar as the environment of the amino terminus free in solution. This is expected if the amino terminus is internalized into the micelle. Thus, the model we propose for hIAPP fragment micelles based on our pH and fluorescence data has the amino terminus incorporated into the interior of the micelle, bringing the amino termini of adjacent peptides into proximity of each other, as well as into a hydrophobic environment, thus resulting in deprotonation of the NH_3^+ groups.

One major area of interest is the characterization of the size of the micelles; however, this has proven to be challenging primarily due to the heterogeneity and small size of these structures and the need to work with low concentrations of the small peptide. Thus, although we were able to visualize the fibrils formed by the hIAPP fragments (by electron microscopy), we were not able to visualize the micelles, which are dynamic, polydisperse structures in rapid equilibrium with monomeric peptide. By their nature, the micelles are sensitive to changes in their environment and may disassemble upon contact with the electron microscopy substrate, due to changes in local monomer concentration. Another classical method for characterizing protein self-association, dynamic light scattering, has also proven inadequate for characterizing the structures formed by hIAPP 20–30. Even at a concentration of $\sim$200 μM hIAPP 20–30 ($\sim$0.22 mg/mL; this concentration is used because, as noted in our previous work—Rhoades et al. (2000)—it is close to highest concentration at which we observe reproducible aggregation and represents the solubility limit of hIAPP 20–30 diluted from DMSO into a neutral aqueous solution) we were unable to obtain a correlation signal for the micelles, indicating that the maximum concentration is still far too low to be detected by light scattering. Additionally, we hypothesize, based on the detection limit of our turbidity studies, that the micelles are composed of not more than 50 monomers, and thus their diffusion may be too rapid to be detected by the correlator.

We show in this work that are able to measure the CMC of hIAPP fragment micelles using techniques well-established for characterizing micellar systems, indicating the potential to use such methods for the study of peptidal systems. It is particularly noteworthy that the CMC value of 3–3.5 μM that we have measured by three independent techniques is in agreement with two of our original observations regarding hIAPP fragment aggregation (Rhoades et al., 2000). First, reproducible, concentration-independent aggregation occurs at concentrations greater than $\sim$5 μM peptide. Second, the critical concentration for hIAPP 20–29 aggregation, C_c, was measured by us to be $\sim$1 μM. Thus, we expect that the CMC should fall in between these measured values, which is indeed where it is found. Current efforts in our lab are being made to characterize the concentration-dependence of hIAPP fragments at sub-CMC concentrations.

References to the in vitro nonfibrillar oligomerization of amyloidogenic proteins have long been found in the literature, describing species ranging in size from dimers to large, amorphous structures (Garzon-Rodriguez et al., 1997; Harper et al., 1997b; Huang et al., 2000; Levine, 1995; Lomakin et al., 1996; Tjernberg et al., 1999; Walsh et al., 1997). However, it is only relatively recently that a possible functional role for amyloid oligomers in amyloid disease pathology has been proposed based on growing evidence from in vivo studies. In particular, these studies have revealed that the toxic forms of several amyloidogenic peptides (including hIAPP) are oligomeric structures, rather than the fully aggregated amyloid fibrils as originally thought (Bhatia et al., 2000; Johnson et al., 1988; Lambert et al., 1998; Zhu et al., 2000). The studies showed that freshly prepared peptide solutions are cytotoxic, indicating the immediate presence of oligomeric species in solution. Earlier studies indicated that the fibrils themselves were the cytotoxic form of amyloid peptides (Fraser et al., 1994; Lorenzo et al., 1994). However, as the importance of nonfibrillar oligomeric species was not recognized at the time, no care was taken to separate this material from the fibrils, and the cytotoxic preparations probably contained a mixture of fibrillar and nonfibrillar oligomers.

Also of interest is a recent study of two mutants of the amyloidogenic protein, α-synuclein, that are linked to early-onset Parkinson's disease (Conway et al., 2000). This study compared the aggregation of these two mutants with the wild-type protein and found that the common property of the mutants was not the rate of fibrillization, but the rate of nonfibrillar oligomerization, which was more rapid for both of the mutants than the wild-type. The studies mentioned above raise the possibility that amyloid fibrils and plaques are relatively harmless products, while the nonfibrillar oligomers cause most of the damage to the cells. If this idea is borne out, therapeutic techniques, which have thus far been aimed at the prevention of fibril formation, may instead focus on preventing the formation of micelles by amyloidogenic peptides.

The present study utilized an amyloidogenic fragment of hIAPP and the question of the biological relevance of a model based on this fragment is an important one. We thus use caution in drawing any conclusions of biological significance based on our simplified in vitro model. As noted in the Introduction, fibrils formed by hIAPP 20–29, as well

as shorter hIAPP fragments within the 20–29 region, are indistinguishable from those formed by full-length hIAPP 1–37 (Ashburn et al., 1992; Azriel and Gazit, 2001; Charge et al., 1995; Glenner et al., 1988; Westermark et al., 1990). Additionally, it was recently shown that preparations of these shorter sequences, hIAPP 22-27 and hIAPP 20-27, as well as hIAPP 20-29, are cytotoxic to rat insulimona cells (Tenidis et al., 2000). Based on these observations, we cannot state with certainty that the aggregation behavior of the fragment is the same as the full-length peptide, but it is clear that it can serve as a useful model in understanding the mechanism underlying amyloidogenesis. It is interesting to note that a number of recent studies of hIAPP and Aβ aimed at inhibiting their aggregation used short, 5–12 amino acid, regions of these peptides with great success (Ghanta et al., 1996; Hughes et al., 2000; Scrocchi et al., 2002; Soto et al., 1996). While evidence accumulates pointing toward nonfibrillar oligomers rather than fibrils as the cytotoxic culprits, raising the question whether preventing amyloid formation is the ultimate goal of therapeutics, all these studies nevertheless demonstrate that the short peptides do provide good target sequences for any studies aimed at understanding, or controlling, the aggregation process.

Despite the great effort put into characterizing the aggregation of amyloidogenic proteins, the process is still not well understood and no kinetic model exists which can serve as a general description of amyloidogenesis. In the present study we present experimental evidence for the formation of micelles by fragments of hIAPP, an observation that strongly supports our previously proposed model for the aggregation of these peptides, which postulates off-pathway peptide micelles. Current efforts in our laboratory aim at further characterization of the micelles as well as obtaining deeper insight into hIAPP fragment aggregation.

REFERENCES

Ashburn, T. T., M. Auger, and P. T. Lansbury. 1992. The structural basis of pancreatic amyloid formation—isotope-edited spectroscopy in the solid state. *J. Am. Chem. Soc.* 114:790–791.

Azriel, R., and E. Gazit. 2001. Analysis of the minimal amyloid-forming fragment of the islet amyloid polypeptide—an experimental support for the key role of the phenylalanine residue in amyloid formation. *J. Biol. Chem.* 276:34156–34161.

Bhatia, R., H. Lin, and R. Lal. 2000. Fresh and globular amyloid beta protein (1–42) induces rapid cellular degeneration: evidence for A-β P-channel-mediated cellular toxicity. *FASEB J.* 14:1233–1243.

Blake, C., and L. Serpell. 1996. Synchrotron x-ray studies suggest that the core of the transthyretin amyloid fibril is a continuous β-sheet helix. *Structure*. 4:989–998.

Blow, D. M., N. E. Chayen, L. F. Lloyd, and E. Saridakis. 1994. Control of nucleation of protein crystals. *Protein Sci.* 3:1638–1643.

Charge, S. B. P., E. J. P. Dekoning, and A. Clark. 1995. Effect of pH and insulin on fibrillogenesis of islet amyloid polypeptide in vitro. *Biochemistry*. 34:14588–14593.

Cohen, A. S., and E. Calkins. 1959. Electron microscopic observations on a fibrous component in amyloid of diverse origins. *Nature*. 183:1202–1203.

Come, J. H., P. E. Fraser, and P. T. Lansbury. 1993. A kinetic-model for amyloid formation in the prion diseases—importance of seeding. *Proc. Natl. Acad. Sci. USA*. 90:5959–5963.

Conway, K. A., S. J. Lee, J. C. Rochet, T. T. Ding, R. E. Williamson, and P. T. Lansbury. 2000. Acceleration of oligomerization, not fibrillization, is a shared property of both α-synuclein mutations linked to early-onset Parkinson's disease: implications for pathogenesis and therapy. *Proc. Natl. Acad. Sci. USA*. 97:571–576.

Cooper, G. J. S., A. C. Willis, A. Clark, R. C. Turner, R. B. Sim, and K. B. M. Reid. 1987. Purification and characterization of a peptide from amyloid-rich pancreases of type 2 diabetic patients. *Proc. Natl. Acad. Sci. USA*. 84:8628–8632.

Cort, J., Z. H. Liu, G. Lee, S. M. Harris, K. S. Prickett, L. S. L. Gaeta, and N. H. Andersen. 1994. β-Structure in human amylin and two designer β-peptides—CD and NMR spectroscopic comparisons suggest soluble β-oligomers and the absence of significant populations of β-strand dimers. *Biochem. Biophys. Res. Commun.* 204:1088–1095.

Dominguez, A., A. Fernandez, N. Gonzalez, E. Iglesias, and L. Montenegro. 1997. Determination of critical micelle concentration of some surfactants by three techniques. *J. Chem. Educ.* 74:1227–1231.

Ferrone, F. A., J. Hofrichter, and W. A. Eaton. 1985. Kinetics of sickle hemoglobin polymerization. I. Studies using temperature jump and laser photolysis techniques. *J. Mol. Biol.* 183:591–610.

Fraser, P. E., D. R. McLachlan, W. K. Surewicz, C. A. Mizzen, A. D. Snow, J. T. Nguyen, and D. A. Kirschner. 1994. Conformation and fibrillogenesis of Alzheimer A-β peptides with selected substitution of charged residues. *J. Mol. Biol.* 244:64–73.

Garzon-Rodriguez, W., M. Sepulveda-Becerra, S. Milton, and C. G. Glabe. 1997. Soluble amyloid A β-(1–40) exists as a stable dimer at low concentrations. *J. Biol. Chem.* 272:21037–21044.

Ghanta, J., C. L. Shen, L. L. Kiessling, and R. M. Murphy. 1996. A strategy for designing inhibitors of β-amyloid toxicity. *J. Biol. Chem.* 271: 29525–29528.

Glenner, G. G., E. D. Eanes, and C. A. Wiley. 1988. Amyloid fibrils formed from a segment of the pancreatic-islet amyloid protein. *Biochem. Biophys. Res. Commun.* 155:608–614.

Goldsbury, C., K. Goldie, J. Pellaud, J. Seelig, P. Frey, S. A. Muller, J. Kistler, G. J. S. Cooper, and U. Aebi. 2000. Amyloid fibril formation from full-length and fragments of amylin. *J. Struct. Biol.* 130:352–362.

Goldsbury, C. S., G. J. S. Cooper, K. N. Goldie, S. A. Muller, E. L. Saafi, W. T. M. Gruijters, and M. P. Misur. 1997. Polymorphic fibrillar assembly of human amylin. *J. Struct. Biol.* 119:17–27.

Griffiths, J. M., T. T. Ashburn, M. Auger, P. R. Costa, R. G. Griffin, and P. T. Lansbury. 1995. Rotational resonance solid-state NMR elucidates a structural model of pancreatic amyloid. *J. Am. Chem. Soc.* 117:3539–3546.

Harper, J. D., C. M. Lieber, and P. T. Lansbury. 1997a. Atomic force microscopic imaging of seeded fibril formation and fibril branching by the Alzheimer's disease amyloid-β protein. *Chem. Biol.* 4:951–959.

Harper, J. D., S. S. Wong, C. M. Lieber, and P. T. Lansbury. 1997b. Observation of metastable A β-amyloid protofibrils by atomic force microscopy. *Chem. Biol.* 4:119–125.

Hiemenz, P. C., and R. Rajogopalan. 1997. Principles of Colloid and Surface Chemistry. Marcel Dekker, Inc., New York.

Huang, T. H. J., D. S. Yang, N. P. Plaskos, S. Go, C. M. Yip, P. E. Fraser, and A. Chakrabartty. 2000. Structural studies of soluble oligomers of the Alzheimer β-amyloid peptide. *J. Mol. Biol.* 297:73–87.

Hughes, E., R. M. Burke, and A. J. Doig. 2000. Inhibition of toxicity in the β-amyloid peptide fragment β-(25–35) using *n*-methylated derivatives —a general strategy to prevent amyloid formation. *J. Biol. Chem.* 275:25109–25115.

Jarrett, J. T., and P. T. Lansbury. 1992. Amyloid fibril formation requires a chemically discriminating nucleation event—studies of an amyloidogenic sequence from the bacterial protein OSMB. *Biochemistry*. 31:12345–12352.

Jarrett, J. T., and P. T. Lansbury. 1993. Seeding one-dimensional crystallization of amyloid—a pathogenic mechanism in Alzheimers disease and scrapie. *Cell*. 73:1055–1058.

Johnson, K. H., T. D. O'Brien, D. W. Hayden, K. Jordan, H. K. G. Ghobrial, W. C. Mahoney, and P. Westermark. 1988. Immunolocalization of islet amyloid polypeptide (IAPP) in pancreatic β-cells by means of peroxidase antiperoxidase (PAP) and protein-A gold techniques. *Am. J. Pathol.* 130:1–8.

Kirschner, D. A., C. Abraham, and D. J. Selkoe. 1986. X-ray diffraction from intraneuronal paired helical filaments and extraneuronal amyloid fibers in Alzheimer disease indicates cross-β conformation. *Proc. Natl. Acad. Sci. USA*. 83:503–507.

Kumar, A. B. M., R. Jayakumar, and K. P. Rao. 1996. Synthesis and aggregational behavior of acidic proteinoid. *J. Polym. Sci. Pol. Chem.* 34:2915–2924.

Lambert, M. P., A. K. Barlow, B. A. Chromy, C. Edwards, R. Freed, M. Liosatos, T. E. Morgan, I. Rozovsky, B. Trommer, K. L. Viola, P. Wals, C. Zhang, C. E. Finch, G. A. Krafft, and W. L. Klein. 1998. Diffusible, nonfibrillar ligands derived from A-β(1–42) are potent central nervous system neurotoxins. *Proc. Natl. Acad. Sci. USA*. 95:6448–6453.

Levine, H. 1995. Soluble multimeric Alzheimer β(1–40) pre-amyloid complexes in dilute solution. *Neurobiol. Aging*. 16:755–764.

Lomakin, A., D. S. Chung, G. B. Benedek, D. A. Kirschner, and D. B. Teplow. 1996. On the nucleation and growth of amyloid β-protein fibrils: detection of nuclei and quantitation of rate constants. *Proc. Natl. Acad. Sci. USA*. 93:1125–1129.

Lomakin, A., D. B. Teplow, D. A. Kirschner, and G. B. Benedek. 1997. Kinetic theory of fibrillogenesis of amyloid β-protein. *Proc. Natl. Acad. Sci. USA*. 94:7942–7947.

Lorenzo, A., B. Razzaboni, G. C. Weir, and B. A. Yankner. 1994. Pancreatic-islet cell toxicity of amylin associated with type 2 *Diabetes Mellitus*. *Nature*. 368:756–760.

Mandal, A. B., and R. Jayakumar. 1994. Aggregation, hydrogen-bonding and thermodynamic studies on tetrapeptide micelles. *J. Chem. Soc. Faraday Trans*. 90:161–165.

Mirchev, R., and F. A. Ferrone. 1997. The structural link between polymerization and sickle cell disease. *J. Mol. Biol.* 265:475–479.

Mukerjee, P., and K. J. Mysels. 1971. Critical Micelle Concentrations of Aqueous Surfactant Systems. National Bureau of Standards, Washington, DC.

Oosawa, F., and M. Kasai. 1962. Theory of linear and helical aggregations of macromolecules. *J. Mol. Biol.* 4:10–23.

Padrick, S. B., and A. D. Miranker. 2002. Islet amyloid: phase partitioning and secondary nucleation are central to the mechanism of fibrillogenesis. *Biochemistry*. 41:4694–4703.

Pallitto, M. M., and R. M. Murphy. 2001. A mathematical model of the kinetics of β-amyloid fibril growth from the denatured state. *Biophys. J.* 81:1805–1822.

Rhoades, E., J. Agarwal, and A. Gafni. 2000. Aggregation of an amyloidogenic fragment of human islet amyloid polypeptide. *Biochim. Biophys. Acta Protein Struct. Mol. Enz.* 1476:230–238.

Schuster, T. M., R. B. Schelle, and L. H. Khairallah. 1979. Mechanism of self-assembly of tobacco mosaic-virus protein. 1. Nucleation-controlled kinetics of polymerization. *J. Mol. Biol.* 127:461–485.

Scrocchi, L. A., Y. Chen, S. Waschuk, F. Wang, S. Cheung, A. A. Darabie, J. McLaurin, and P. E. Fraser. 2002. Design of peptide-based inhibitors of human islet amyloid polypeptide fibrillogenesis. *J. Mol. Biol.* 318: 697–706.

Serio, T. R., A. G. Cashikar, A. S. Kowal, G. J. Sawicki, J. J. Moslehi, L. Serpell, M. F. Arnsdorf, and S. L. Lindquist. 2000. Nucleated conformational conversion and the replication of conformational information by a prion determinant. *Science*. 289:1317–1321.

Snyder, S. W., U. S. Ladror, W. S. Wade, G. T. Wang, L. W. Barrett, E. D. Matayoshi, H. J. Huffaker, G. A. Krafft, and T. F. Holzman. 1994. Amyloid-β aggregation—selective inhibition of aggregation in mixtures of amyloid with different chain lengths. *Biophys. J.* 67:1216–1228.

Soto, C., M. S. Kindy, M. Baumann, and B. Frangione. 1996. Inhibition of Alzheimer's amyloidosis by peptides that prevent β-sheet conformation. *Biochem. Biophys. Res. Commun.* 226:672–680.

Sunde, M., L. C. Serpell, M. Bartlam, P. E. Fraser, M. B. Pepys, and C. C. F. Blake. 1997. Common core structure of amyloid fibrils by Synchrotron x-ray diffraction. *J. Mol. Biol.* 273:729–739.

Tenidis, K., M. Waldner, J. Bernhagen, W. Fischle, M. Bergmann, M. Weber, M. L. Merkle, W. Voelter, H. Brunner, and A. Kapurniotu. 2000. Identification of a penta- and hexapeptide of islet amyloid polypeptide (IAPP) with amyloidogenic and cytotoxic properties. *J. Mol. Biol.* 295:1055–1071.

Tjernberg, L. O., A. Pramanik, S. Bjorling, P. Thyberg, J. Thyberg, C. Nordstedt, K. D. Berndt, L. Terenius, and R. Rigler. 1999. Amyloid β-peptide polymerization studied using fluorescence correlation spectroscopy. *Chem. Biol.* 6:53–62.

Tomski, S. J., and R. M. Murphy. 1992. Kinetics of aggregation of synthetic β-amyloid peptide. *Arch. Biochem. Biophys.* 294:630–638.

Walsh, D. M., D. M. Hartley, Y. Kusumoto, Y. Fezoui, M. M. Condron, A. Lomakin, G. B. Benedek, D. J. Selkoe, and D. B. Teplow. 1999. Amyloid-β protein fibrillogenesis—structure and biological activity of protofibrillar intermediates. *J. Biol. Chem.* 274:25945–25952.

Walsh, D. M., A. Lomakin, G. B. Benedek, M. M. Condron, and D. B. Teplow. 1997. Amyloid β-protein fibrillogenesis—detection of a protofibrillar intermediate. *J. Biol. Chem.* 272:22364–22372.

Westermark, P., U. Engstrom, K. H. Johnson, G. T. Westermark, and C. Betsholtz. 1990. Islet amyloid polypeptide—pinpointing amino-acid residues linked to amyloid fibril formation. *Proc. Natl. Acad. Sci. USA*. 87:5036–5040.

Westermark, P., and E. Wilander. 1978. Influence of amyloid deposits on islet volume in maturity onset *Diabetes Mellitus*. *Diabetologia*. 15:417–421.

Wood, S. J., B. Maleeff, T. Hart, and R. Wetzel. 1996. Physical, morphological and functional differences between pH 5.8 and 7.4 aggregates of the Alzheimer's amyloid peptide AP. *J. Mol. Biol.* 256:870–877.

Zhu, Y. J., H. Lin, and R. Lal. 2000. Fresh and nonfibrillar amyloid beta protein (1–40) induces rapid cellular degeneration in aged human fibroblasts: evidence for A β P-channel-mediated cellular toxicity. *FASEB J.* 14:1244–1254.